International Journal of Solids and Structures 180–181 (2019) 84–96

Contents lists available at ScienceDirect

International Journal of Solids and Structures

journal homepage: www.elsevier.com/locate/ijsolstr

Constitutive modeling of anisotropic plasticity with application to fiber-reinforced composites

Swaroop G Nagaraja, Martin Pletz, Clara Schuecker*

Chair of Designing Plastics and Composite Materials, Department of Polymer Engineering and Science, Montanuniversitaet Leoben, Austria

ARTICLE INFO

Article history:
Received 28 February 2019
Revised 25 June 2019
Accepted 1 July 2019
Available online 4 July 2019

Keywords:
Fiber-reinforced composites
Anisotropy
Plasticity theory

ABSTRACT

This article proposes two constitutive models to describe the nonlinear, elastic-plastic behavior of unidirectional fiber-reinforced composites at the meso-level. Key ingredients are the formulation of two anisotropic yield functions with the aid of representation theorems (invariant formulation), and the set-up of governing equations for plastic variables with respect to associative and non-associative flow response. The governing equations are solved using an elastic predictor-plastic corrector algorithm which imposes the constraint posed by the yield condition. Both the models are evaluated qualitatively and quantitatively by comparison to micromechanics simulations as well as to experimental data.

© 2019 Elsevier Ltd. All rights reserved.

1. Introduction

With the increasing use of unidirectional fiber-reinforced composites as a primary structural component in the automobile and aerospace industries, the predictive modeling of the non-linear behavior of composites has been a topic of intensive research over the last years. From an experimental perspective, investigations pertaining to the non-linear behavior of composites are documented in (Smith, 2000; Vogler and Kyriakides, 1998; 1999; Weeks and Sun, 1995), among others. It has been observed that the material response of the composite to shear and transverse compression is non-linear and inelastic whereas that in the fiber direction remains essentially elastic up to failure. Due to the brittle behavior of polymers used in composites, it is usually assumed that the non-linearity is a result of brittle cracking inside the matrix material only. Therefore, previous modeling efforts have emphasized on continuum damage mechanics (Rabotnov, 1969; Lemaitre, 1992). Recent research implies that under shear dominated loads, considerable permanent strains develop that cannot be explained by brittle mechanisms alone. It has been experimentally observed (Gilat et al., 2005; G'sell et al., 1990) and computationally verified (Schuecker and Pettermann, 2008) that the non-linearity is due to plasticity in the matrix constituent. Moreover, plasticity prior to damage leads to a redistribution of the stress state in a laminate, which eventually affects the failure onset. Therefore, accurate constitutive models which capture the elastic-plastic behavior of these materials are required to accurately predict the onset of damage and failure of composite materials (Chang and Chang, 1987).

Generally, the elastic-plastic behavior of composite materials can be described using either a *micromechanical* or a *homogenized* approach. Along the lines of a *micromechanical* approach, fibers and the matrix are modeled as individual phases. Fibers are assumed to be linear elastic anisotropic solids (as necessary for carbon fibers) whereas the matrix is modeled as an isotropic elastic-plastic solid, see (Pettermann et al., 1993; Hsu et al., 1999; Doghri and Ouaar, 2003; Doghri et al., 2010) for details regarding the constitutive and algorithmic framework. The micromechanical approach gives a better understanding of reasons behind the behavior observed in experiments. However, this approach comes at a cost where higher number of material coefficients are required for the description of material response. Although differing in detail with the micromechanical approach, a small number of constitutive models of anisotropic plasticity, based on a linear transformation of the stress tensor have been proposed, see (Car et al., 2000; 2001), with emphasis on fiber-reinforced composites. This theory assumes the existence of a fictitious isotropic space where a mapped problem is solved. The real and fictitious spaces are related by means of linear fourth-order transformation tensors which are formulated based on the available information of strength in the respective spaces. The real anisotropic space is regarded as a homogenized composite material while the fictitious isotropic space characterizes the matrix material to which plasticity is usually restricted.

A majority of relevant research has focused on the formulation and experimental validation of anisotropic yield criteria for *homogenized* models. Hill (1950) proposed one of the first yield functions for the description of orthotropy, which is a generalization

* Corresponding author.
E-mail address: Clara.Schuecker@unileoben.ac.at (C. Schuecker).

https://doi.org/10.1016/j.ijsolstr.2019.07.002
0020-7683/© 2019 Elsevier Ltd. All rights reserved.

of the Mises (1928) isotropic yield criterion. The main limitation of this criterion is the impossibility of modeling materials that exhibit pressure sensitive behavior, i.e. composite materials, following which there have been attempts to modify Hill's orthotropic yield criterion for use with unidirectional composites (Xie and Adams, 1995; Sun and Chen, 1989; Chen and Sun, 1993). For metal-matrix composites, there are a considerable number of thermodynamically consistent models for the description of anisotropic elastic-plastic effects, see e.g., Dvorak and Bahei-El-Din (1987), Rogers (1987), Spencer (1992), Voyiadjis and Thiagarajan (1995), Voyiadjis and Thiagarajan (1996), Smith et al. (2015). The review article of Chaboche (2008) thoroughly treats the formulation and implementation aspects of elastoplasticity for metallic-type materials. However, the treatment of anisotropic plasticity for polymer-matrix composites is in most cases limited to a purely phenomenological approach (Flatscher et al., 2013; Maimí et al., 2011; Al-Haik et al., 2004), and constitutive modeling using the thermodynamics of irreversible processes has received less attention (Tsai and Sun, 2002; Kontou and Spathis, 2006; Vyas et al., 2011; Vogler et al., 2013). Additionally, none of the aforementioned works for polymer-matrix composites use functional forms of hardening state variables within a thermodynamically consistent formulation.

Motivated by these aspects, the goal of this paper is to outline a relatively general, thermodynamically consistent formulation of anisotropic elastoplasticity, with application to polymer composites reinforced by unidirectional fibers. Two constitutive models are formulated based on the following main ideas:

- The objective of the proposed constitutive models ultimately is their application to modeling uni-directional plies in multi-directional laminates. In such materials, plasticity formulations are primarily needed to accurately predict the constitutive response up to initiation of matrix damage, which typically occurs at rather low strains (below 1%). In view of this objective, the constitutive models are formulated in the framework of small strains. Even though simulations are performed up to 4% strain, deviations are considered to be acceptable for the purpose of comparing various modeling techniques (Hsu et al., 1999).
- The methodology adopted here is to generate the constitutive functions representing the elastic-plastic response with the aid of representation theorems. This approach allows for the formulation of anisotropic constitutive functions in terms of isotropic counterparts by including structural tensors as additional arguments (Boehler, 1979; Liu, 1982; Zheng and Spencer, 1993). In this context, a new integrity basis is derived, that yields a unique representation of the scalar energetic potential, the stress and the elastic modulus tensor associated with the potential.
- A simplifying assumption made at the outset, due to the restriction to geometrical linear theory, is that the anisotropy does not evolve during the plastic deformation. Details related to the modeling of an evolving anisotropy can be found in (Miehe, 1998). Furthermore, the focus is restricted to transversely isotropic symmetry group which characterizes unidirectional fiber-reinforced composites.
- The effects associated with the interface between the fibers and the matrix are not considered, as they are usually observed at large deformations (Totry et al., 2008; 2010).
- The formulation of plastic response functions is based on a physically motivated decomposition of the stress tensor (Spencer, 1992), which ensures a linear elastic fiber response. Two non-quadratic yield functions with non-linear isotropic hardening are proposed, with a simple representation in terms of the invariants of the stress tensor. Non-quadratic yield functions are chosen in order to maintain the same order of the stress invariants. It should be remarked here that though higher order yield functions are accurate (Vogler et al., 2013), they require higher number of coefficients which must be obtained experimentally (Cordoso and Adetoro, 2017). The main advantage of the proposed yield functions is that they are governed by only three anisotropic coefficients, and they accurately predict the trends of experimentally observed behavior when combined with an associated flow rule. An assessment of these two models reveals that the predictions are more accurate for lower values of the anisotropic coefficient governing the hydrostatic pressure. Moreover, the conditions for the convexity of the proposed yield surfaces are simple to derive and impose, as seen in Appendix A. One of the yield surfaces is conditionally valid where a certain inequality governs its convexity, while the other has no such restrictions.
- Next, the algorithmic treatment of the constitutive models is presented, where the resulting differential and algebraic equations of the plastic flow are solved using an implicit time integration scheme (Simó and Hughes, 2000). This is followed by a detailed discussion on the methodology designed to calibrate constitutive models so that they accurately reproduce the experimental response. Numerical simulations which serve the purpose of evaluating the models qualitatively and quantitatively are presented at the end.

2. Constitutive framework

In this section, constitutive equations describing the transversely isotropic elastic-plastic response are formulated in an invariant setting, using the representation theorems of tensor functions. The constitutive relations derived are based on the following form of the Clausius-Planck inequality for isothermal conditions

$$\mathcal{D} = \boldsymbol{\sigma} : \dot{\boldsymbol{\varepsilon}} - \dot{\Psi} \geq 0 \tag{1}$$

which defines the local dissipation $\mathcal{D}$ of the model per unit volume as a function of the stress $\boldsymbol{\sigma}$, the overall strain $\boldsymbol{\varepsilon}$, and the free energy function per unit volume Ψ, see Simó and Hughes (2000, Chapter 1, Section 1.3.3, pp. 27) for details. The free energy function is assumed to be of the form

$$\Psi = \Psi(\boldsymbol{\varepsilon} - \boldsymbol{\varepsilon}^p, \alpha) \tag{2}$$

in terms of a suitable set $\{\boldsymbol{\varepsilon}^p, \alpha\}$ of internal variables. Here, $\boldsymbol{\varepsilon}^p$ is a second-order tensor denoting the *plastic strain* and α is a phenomenological *hardening variable* that characterizes isotropic hardening. Substituting (2) into (1) and applying Coleman's exploitation method gives the constitutive law for the stress tensor $\boldsymbol{\sigma}$ and driving forces $\{\boldsymbol{\sigma}^p, \beta\}$ as

$$\begin{aligned} \boldsymbol{\sigma} &= \partial_{(\boldsymbol{\varepsilon}-\boldsymbol{\varepsilon}^p)} \Psi(\boldsymbol{\varepsilon} - \boldsymbol{\varepsilon}^p, \alpha) \\ \boldsymbol{\sigma}^p &= -\partial_{\boldsymbol{\varepsilon}^p} \Psi(\boldsymbol{\varepsilon} - \boldsymbol{\varepsilon}^p, \alpha) \\ \beta &= -\partial_{\alpha} \Psi(\boldsymbol{\varepsilon} - \boldsymbol{\varepsilon}^p, \alpha), \end{aligned} \tag{3}$$

see Miehe et al. (2002) for details. As a consequence of the geometrically linear theory, it follows that $\boldsymbol{\sigma}^p = \boldsymbol{\sigma}$. Insertion of (3) into (1) gives the reduced dissipation inequality

$$\mathcal{D} = \boldsymbol{\sigma} : \dot{\boldsymbol{\varepsilon}}^p + \beta \dot{\alpha} \geq 0. \tag{4}$$

The equation above represents the restriction imposed by the second axiom of thermodynamics which demands that the dissipation always be non-negative. In what follows, explicit forms of the free energy function and the yield function are derived with the aid of representation theorems for the transversely isotropic symmetry group.

2.1. Invariant formulation of transverse isotropy

Let $\boldsymbol{a}$ be a positively oriented vector denoting the preferred direction, such that the symmetry group can be fully described by rotations and reflections relative to this vector. The *symmetry group* $\mathscr{C}$ of the considered transversely isotropic material is identified by a set of orthogonal transformations $\boldsymbol{Q}$, i.e.

$$\mathscr{C} = \{\boldsymbol{Q}_{\parallel\boldsymbol{a}}, \boldsymbol{Q}^{\pi}_{\perp\boldsymbol{a}}\} \subset \mathcal{O}(3) \quad \text{with} \quad \mathcal{O}(3) := \{\boldsymbol{Q} | \boldsymbol{Q}^T\boldsymbol{Q} = \boldsymbol{1} \;\&\; \det[\boldsymbol{Q}] = 1\}, \tag{5}$$

where $\boldsymbol{Q}_{\parallel\boldsymbol{a}}$ are arbitrary rotations relative to the vector $\boldsymbol{a}$, $\boldsymbol{Q}^{\pi}_{\perp\boldsymbol{a}}$ are rotations about a vector perpendicular to $\boldsymbol{a}$ by the angle π, $\mathcal{O}(3)$ is the set of orthogonal transformations and $\boldsymbol{1}$ is the second-order identity tensor. The principle of material symmetry strongly restricts the free energy function (2) and demands invariance such that

$$\Psi(\boldsymbol{Q}(\boldsymbol{\varepsilon} - \boldsymbol{\varepsilon}^p)\boldsymbol{Q}^T, \alpha) = \Psi(\boldsymbol{\varepsilon} - \boldsymbol{\varepsilon}^p, \alpha) \quad \forall \boldsymbol{Q} \in \mathscr{C}, \tag{6}$$

which indicates Ψ is a transversely isotropic scalar function, see Lu and Zhang (2005). In view of a coordinate free formulation, it has been proven in (Boehler, 1979) that such an anisotropic function (6) can be expressed as an isotropic function with an extended set of arguments denoted as *structural tensors*. Furthermore, it has been established in (Boehler, 1979; Zheng and Spencer, 1993) that transverse isotropy is fully characterized by a single second-order structural tensor $\boldsymbol{m}$, expressed as

$$\boldsymbol{m} := \boldsymbol{a} \otimes \boldsymbol{a} \quad \text{with} \quad \boldsymbol{Q}\boldsymbol{m}\boldsymbol{Q}^T = \boldsymbol{m} \quad \forall \boldsymbol{Q} \in \mathscr{C}. \tag{7}$$

Appealing to the representation theorem for isotropic scalar- and tensor-valued functions of the arguments $(\boldsymbol{\varepsilon} - \boldsymbol{\varepsilon}^p)$ and $\boldsymbol{m}$, an irreducible integrity basis for scalar functions of a transversely isotropic response, consists of the following invariants

$$I_1 = \mathrm{tr}[\boldsymbol{\varepsilon} - \boldsymbol{\varepsilon}^p], \quad I_2 = \mathrm{tr}[(\boldsymbol{\varepsilon} - \boldsymbol{\varepsilon}^p)^2], \quad I_3 = \mathrm{tr}[(\boldsymbol{\varepsilon} - \boldsymbol{\varepsilon}^p)^3],$$
$$I_4 = \mathrm{tr}[\boldsymbol{m}(\boldsymbol{\varepsilon} - \boldsymbol{\varepsilon}^p)] \quad \text{and} \quad I_5 = \mathrm{tr}[\boldsymbol{m}(\boldsymbol{\varepsilon} - \boldsymbol{\varepsilon}^p)^2] \tag{8}$$

see Zheng (1994). Based on (8), a new integrity basis is introduced that will yield a unique representation of the free energy function, the stress associated with the free energy function and the elastic modulus. This basis is constructed by reformulating the isotropic invariants of the elastic strain $(\boldsymbol{\varepsilon} - \boldsymbol{\varepsilon}^p)$ as follows

$$\mathrm{tr}[\boldsymbol{\varepsilon} - \boldsymbol{\varepsilon}^p] = \mathrm{tr}[\boldsymbol{m}(\boldsymbol{\varepsilon} - \boldsymbol{\varepsilon}^p)] + \mathrm{tr}[(\boldsymbol{1} - \boldsymbol{m})(\boldsymbol{\varepsilon} - \boldsymbol{\varepsilon}^p)] \quad \text{and}$$
$$\frac{1}{2}\mathrm{tr}[(\boldsymbol{\varepsilon} - \boldsymbol{\varepsilon}^p)^2] = \mathrm{tr}[\boldsymbol{m}(\boldsymbol{\varepsilon} - \boldsymbol{\varepsilon}^p)^2] + \mathrm{tr}[(\frac{1}{2}\boldsymbol{1} - \boldsymbol{m})(\boldsymbol{\varepsilon} - \boldsymbol{\varepsilon}^p)^2]. \tag{9}$$

Substituting (9) in (8) and replacing $\mathrm{tr}[(\boldsymbol{\varepsilon} - \boldsymbol{\varepsilon}^p)^3]$ by $\det[\boldsymbol{\varepsilon} - \boldsymbol{\varepsilon}^p]$ using the Cayley–Hamilton's theorem, the new integrity basis reads

$$\tilde{I}_1 = \mathrm{tr}[\boldsymbol{m}(\boldsymbol{\varepsilon} - \boldsymbol{\varepsilon}^p)], \quad \tilde{I}_2 = \mathrm{tr}[(\boldsymbol{1} - \boldsymbol{m})(\boldsymbol{\varepsilon} - \boldsymbol{\varepsilon}^p)],$$
$$\tilde{I}_3 = \mathrm{tr}[\boldsymbol{m}(\boldsymbol{\varepsilon} - \boldsymbol{\varepsilon}^p)^2],$$
$$\tilde{I}_4 = \mathrm{tr}\left[\left(\frac{1}{2}\boldsymbol{1} - \boldsymbol{m}\right)(\boldsymbol{\varepsilon} - \boldsymbol{\varepsilon}^p)^2\right] \quad \text{and} \quad \tilde{I}_5 = \det[\boldsymbol{\varepsilon} - \boldsymbol{\varepsilon}^p] \tag{10}$$

where the first two modes in (10) are normal and the next two modes are shear. In the remainder of this article, the cubic invariants are neglected as they are most suitable for modeling the plastic response of metallic-type materials. The scalar free energy function can now be constructed by taking combinations of the invariants defined above and assuming appropriate hardening rules.

2.2. Elastic response functions

A *quadratic* free energy function Ψ can be written with the aid of (10) as

$$\Psi = \frac{\mu_1}{2}\tilde{I}_1^2 + \frac{\mu_2}{2}\tilde{I}_2^2 + \mu_3\tilde{I}_1\tilde{I}_2 + 2\mu_4\tilde{I}_3 + 2\mu_5\tilde{I}_4 + \Psi(\alpha) \tag{11}$$

where μ_{1-5} are five independent Lamé parameters required to describe the transversely isotropic response. A prescription for the identification of Lamé parameters in terms of engineering constants suggested in (Schröder et al., 2002) has been used in this work.

Power law based isotropic hardening is incorporated by defining the function $\Psi(\alpha)$ as

$$\Psi(\alpha) = \frac{h}{n+1}(\bar{\alpha} + \alpha)^{n+1} \tag{12}$$

where h is the hardening modulus, $n > 0$ is the hardening exponent, and $\bar{\alpha}$ is a parameter describing prestrain, which is necessary for numerical reasons and is set to a very low value such that it has negligible effect on the results.

2.3. Plastic response functions

As a main characteristic of the elastic-plastic material response, an elastic domain $\mathscr{S}$ is assumed, defined by

$$\mathscr{S} = \{(\boldsymbol{\sigma}, \beta) \in \mathbb{R}^6 \times \mathbb{R} | \chi(\boldsymbol{\sigma}, \boldsymbol{m}, \beta) \leq 0\}, \tag{13}$$

where $\chi = \chi(\boldsymbol{\sigma}, \boldsymbol{m}, \beta)$ is the yield function in the admissible stress space. The yield function can also be expressed as an isotropic scalar function such that

$$\chi(\boldsymbol{Q}\boldsymbol{\sigma}\boldsymbol{Q}^T, \boldsymbol{Q}\boldsymbol{m}\boldsymbol{Q}^T, \beta) = \chi(\boldsymbol{\sigma}, \boldsymbol{m}, \beta) \quad \forall \boldsymbol{Q} \in \mathcal{O}(3). \tag{14}$$

The two yield functions formulated subsequently, are based on the definition of a plasticity inducing stress $\mathfrak{s}$, originally introduced by Spencer (1992) in the context of formulating plastic response functions for unidirectional fiber-reinforced composites. According to Spencer (1992), the second-order tensor $\mathfrak{s}$ is required to be *deviatoric* and *stress free in the fiber direction* such that

$$\mathrm{tr}[\mathfrak{s}] = 0 \quad \text{and} \quad \mathrm{tr}[\boldsymbol{m}\mathfrak{s}] = 0. \tag{15}$$

These two conditions allow for the definition of $\mathfrak{s}$, for a given fiber direction $\boldsymbol{m}$, as

$$\mathfrak{s} = \boldsymbol{\sigma} - \frac{1}{3}\mathrm{tr}[\boldsymbol{\sigma}]\boldsymbol{1} - \frac{3}{2}\mathrm{tr}[\boldsymbol{m}'\boldsymbol{\sigma}]\boldsymbol{m}' \quad \text{with} \quad \boldsymbol{m}' = \boldsymbol{m} - \frac{1}{3}\boldsymbol{1}, \tag{16}$$

see also Lu and Zhang (2005). With the preceding definitions in place, two pressure-dependent, threshold-type yield functions are proposed that are suitable for unidirectional fiber-reinforced composites. The underlying difference is the condition for their convexity which is elaborated subsequently.

2.3.1. Model-I

Analogous to (8), the integrity basis for the formulation of the yield function χ in terms of argument tensors $\mathfrak{s}$ and $\boldsymbol{m}$, taking (15) into account, consists of the invariants

$$J_1 = \mathrm{tr}[\boldsymbol{\sigma}], \quad J_2 = \mathrm{tr}[\mathfrak{s}^2], \quad J_3 = \mathrm{tr}[\mathfrak{s}^3], \quad J_4 = \mathrm{tr}[\boldsymbol{m}\boldsymbol{\sigma}] \quad \text{and}$$
$$J_5 = \mathrm{tr}[\boldsymbol{m}\mathfrak{s}^2] \tag{17}$$

see also Spencer (1992). In line with (9), the linear and quadratic isotropic invariants in (17) can be reformulated as

$$\mathrm{tr}[\boldsymbol{\sigma}] = \mathrm{tr}[\boldsymbol{m}\boldsymbol{\sigma}] + \mathrm{tr}[(\boldsymbol{1} - \boldsymbol{m})\boldsymbol{\sigma}] \quad \text{and}$$
$$\mathrm{tr}[\mathfrak{s}^2] = \mathrm{tr}[\boldsymbol{m}\mathfrak{s}^2 + \mathfrak{s}^2\boldsymbol{m}] + \mathrm{tr}[\mathfrak{s}^2 - (\boldsymbol{m}\mathfrak{s}^2 + \mathfrak{s}^2\boldsymbol{m})]. \tag{18}$$

It should be noted that the reformulation of quadratic invariants in $(18)_2$ is slightly different from that in $(9)_2$. This particular form of quadratic invariants has been chosen because the plastic response functions formulated subsequently using these invariants, are found to capture the observed experimental behavior quite well, as seen in the later part of this paper. Substituting (18) into (17) and replacing $\mathrm{tr}[\mathfrak{s}^3]$ by $\det[\mathfrak{s}]$ using the Cayley–Hamilton's theorem, the new integrity basis reads

$$\tilde{J}_1 = \mathrm{tr}[(\boldsymbol{1}-\boldsymbol{m})\boldsymbol{\sigma}],\ \tilde{J}_2 = \mathrm{tr}[\boldsymbol{m}\mathfrak{s}^2+\mathfrak{s}^2\boldsymbol{m}],\ \tilde{J}_3 = \mathrm{tr}[\mathfrak{s}^2-(\boldsymbol{m}\mathfrak{s}^2+\mathfrak{s}^2\boldsymbol{m})],$$
$$\tilde{J}_4 = \mathrm{tr}[\boldsymbol{m}\boldsymbol{\sigma}] \quad \text{and} \quad \tilde{J}_5 = \det[\mathfrak{s}]. \tag{19}$$

The linear invariants $\tilde{J}_1$ and $\tilde{J}_4$ characterize the two normal modes, namely the hydrostatic pressure in transverse and fiber direction, respectively, and the quadratic invariants $\tilde{J}_2$ and $\tilde{J}_3$ characterize the two shear modes, denoting the in-plane and transverse shear, respectively. An advantage of using the plasticity inducing stress tensor $\mathfrak{s}$ for the definition of quadratic invariants in (17) is the resulting decoupled representation of the shear stress as defined above. As a consequence, parameter identification is significantly simplified. With the basis (19) at hand, the plastic response function can be defined analogous to the elastic response function (11), however, the following aspects help towards the precise development of the yield function, in the context of modeling the inelastic response of polymeric composites:

1. For polymeric composites, the plastic response is independent of stress in the fiber direction (Vogler et al., 2013).
2. The plastic response function should be pressure-dependent as the yield behavior of polymers is significantly affected by the hydrostatic pressure (Colak, 2005).
3. Plastic yielding should be governed by limited number of coefficients.

Taking into to account these aspects, the yield function for Model-I, which can be regarded as an analogue of the classical isotropic Drucker–Prager pressure-dependent yield function, is proposed as

$$\chi = \eta_1\tilde{J}_1 + \left[\eta_2\tilde{J}_2+\eta_3\tilde{J}_3\right]^{1/2} - \left(1-\frac{\beta}{y_{12}}\right) \leq 0 \tag{20}$$

where η_{1-3} are material parameters governing the transversely isotropic plastic yielding. These parameters are related to the compressive yield stress y_{22c}, in-plane shear yield stress y_{12} and transverse shear yield stress y_{23} respectively. They are determined by the evaluation of the yield function (20) for one compression and two shear modes, with $\boldsymbol{a} = [1,0,0]^T$ and $\beta = 0$ Schröder et al. (2002), as

$$\eta_1 = \frac{1}{2y_{23}} - \frac{1}{y_{22c}}, \quad \eta_2 = \frac{1}{2y_{12}^2} \quad \text{and} \quad \eta_3 = \frac{1}{2y_{23}^2}. \tag{21}$$

Convexity of the yield function is a necessary requirement for minimization problems in order to have a unique solution (Drucker, 1964). It ensures the dissipation to remain positive for all admissible thermodynamic processes, which is the central idea of the second axiom of thermodynamics. For the particular model at hand, the inequality $\eta_3 \geq \eta_2$, i.e. $y_{12} \geq y_{23}$ must be true for the yield surface (20) to be convex (see Appendix A for proof). This restriction serves as a motivation for the subsequent Model-II.

2.3.2. Model-II

In order to overcome the restriction imposed by the convexity condition of the Model-I, use is made of the Euclidean norm in the context of defining the second yield function. To this end, a further decomposition of the plasticity inducing stress tensor $\mathfrak{s}$ into two distinct shear terms denoting the in-plane and transverse stresses is considered such that

$$\mathfrak{s}_2 = \boldsymbol{m}\mathfrak{s} + \mathfrak{s}\boldsymbol{m} \quad \text{and} \quad \mathfrak{s}_3 = \mathfrak{s} - (\boldsymbol{m}\mathfrak{s} + \mathfrak{s}\boldsymbol{m}). \tag{22}$$

see also Lu and Zhang (2005). The decomposition above is an extension of the additive stress split introduced in (Spencer, 1992), and facilitates a unique way to the formulation of the yield function.

Let p denote the hydrostatic pressure such that

$$p = \mathrm{tr}[(\boldsymbol{1}-\boldsymbol{m})\boldsymbol{\sigma}]. \tag{23}$$

Appealing to (22) and (23), a Drucker–Prager-type pressure-dependent yield function is proposed in the stress space as

$$\chi = \eta_1 p + \left[\eta_2\|\mathfrak{s}_2\|^2 + \eta_3\|\mathfrak{s}_3\|^2\right]^{1/2} - \left(1-\frac{\beta}{y_{12}}\right) \leq 0 \tag{24}$$

where $\|\cdot\|$ denotes the Euclidean norm of a second-order tensor, see also Papadopoulos and Lu (2001). Analogous to Model-I, the yield surface parameters are evaluated to be

$$\eta_1 = \frac{1}{\sqrt{2}y_{23}} - \frac{1}{y_{22c}}, \quad \eta_2 = \frac{1}{y_{12}^2} \quad \text{and} \quad \eta_3 = \frac{1}{y_{23}^2}. \tag{25}$$

Taking into account the fact that the Hessian of the squared Euclidean norm is the identity matrix, which is positive definite, the requirement for convexity of the yield function (24) is given by $\eta_2 > 0$ and $\eta_3 > 0$ (cf. to Naghdi-Trapp inequality Naghdi and Trapp, 1975; Casey, 1984), which is generally fulfilled by (25).

2.3.3. Evolution of internal variables

Taking into account (11) and (20)/(24), the generalized *normality rules* (Lubliner, 1997; Aldakheel and Miehe, 2017) which define the evolution equations for the plastic variables take the form

$$\dot{\boldsymbol{\varepsilon}}^p = \lambda\partial_{\boldsymbol{\sigma}}\chi \quad \text{and} \quad \dot{\alpha} = \lambda\partial_{\beta}\chi \tag{26}$$

which are supplemented by plastic loading-unloading conditions

$$\lambda \geq 0,\ \chi \leq 0 \quad \text{and} \quad \lambda\chi = 0. \tag{27}$$

Here, λ is the plastic multiplier determined by the consistency condition $\dot{\chi} = 0$. Evolution laws of type (26) are referred to as *associated flow* rules and are characterized by the fact that the rates of the internal variables are normal to the yield surface ($\chi = 0$).

In situations where the canonical normal directions of the evolution equations (26) do not characterize the real material response, i.e. *non-associative* flow, the constitutive response is modified by introducing an additional constitutive function Φ, referred to in what follows as the plastic flow potential. It is assumed to depend on the same variables as the yield function (20)/(24) such that

$$\Phi = \Phi(\boldsymbol{\sigma}, \boldsymbol{m}, \beta) \tag{28}$$

based on which the evolution equations for the plastic variables take the form

$$\dot{\boldsymbol{\varepsilon}}^p = \lambda\partial_{\boldsymbol{\sigma}}\Phi \quad \text{and} \quad \dot{\alpha} = \lambda\partial_{\beta}\Phi. \tag{29}$$

Note that (29) replaces the normality rules in (26), though the plastic loading conditions remain unchanged. In the present work, a plastic flow potential of the form

$$\Phi = \chi\,|_{\eta_1=0} \tag{30}$$

is considered, such that (29) is independent of the hydrostatic pressure and fiber stress.

It should be emphasized here that the proposed plastic response functions (20) and (30) in the present work differs from that in (Vogler et al., 2013) in two aspects. Firstly, the number of anisotropic coefficients governing the yield function in (20) is significantly less. Secondly, the evolution of hardening variable in the present work is formally derived by invoking and relaxing the principle of maximum dissipation, with respect to the associative and non-associative plasticity, respectively, and assumed to be $\dot{\alpha} = \sqrt{\frac{1}{2}\|\dot{\boldsymbol{\varepsilon}}^p\|}$ in (Vogler et al., 2013). Furthermore, to the knowledge of the authors, the use of the pressure-dependent, transversely isotropic yield function (24), in combination with a pressure-independent plastic flow potential (30) to constitutively frame the model within non-associative plasticity is novel, and has been pointed out here for the first time, with application to polymeric composites.

Remark 1. Normally, the plastic flow potential should be determined based on the experimental observations, where the direction of the plastic flow shows significant deviations from the direction of the normal to the yield surface (Dvorak et al., 1988). This non-associativity of plastic strains has been investigated in (Voyiadjis and Thiagarajan, 1995), with emphasis on metal-matrix composites. However, due to the lack of experimental data for polymer-matrix composites, a plastic flow potential of the form (30) is considered, following conceptually (Hsu et al., 1999; Mosler and Bruhns, 2009).

3. Algorithmic implementation

In this section, aspects of the algorithmic implementation of the proposed plasticity models are discussed. In particular, the focus is on the numerical integration of the set of constitutive equations developed in Section 2. The algorithmic treatment is in the spirit of predictor-corrector method, widely used for implicit simulations. A detailed discussion of the relevant literature is provided in the monograph of Simó and Hughes (2000).

At first, the evolution laws are approximated by a backward Euler time integration scheme in a finite time step $[t_{n+1}, t_n]$, with $\Delta t := t_{n+1} - t_n$. To have a compact notation, all variables without a subscript are meant to be evaluated at time t_{n+1}. Thus, Eqs. (26) and (29) are integrated as

$$\left.\begin{aligned} \boldsymbol{\varepsilon}^p &= \boldsymbol{\varepsilon}^p_n + \gamma\, \partial_{\boldsymbol{\sigma}} \chi \\ \alpha &= \alpha_n + \gamma\, \partial_\beta \chi \end{aligned}\right\} \quad \text{and} \quad \left.\begin{aligned} \boldsymbol{\varepsilon}^p &= \boldsymbol{\varepsilon}^p_n + \gamma\, \partial_{\boldsymbol{\sigma}} \Phi \\ \alpha &= \alpha_n + \gamma\, \partial_\beta \Phi \end{aligned}\right\} \tag{31}$$

with $\gamma = \Delta t \lambda$ denoting the plastic increment. With (31), it follows from (3), and the consistency condition $\chi = 0$, that the related system of equations can be grouped into a residual vector $\mathscr{R}$ as

$$\mathscr{R} = \begin{bmatrix} \mathscr{R}_{\boldsymbol{\sigma}} \\ \mathscr{R}_\beta \\ \mathscr{R}_\chi \end{bmatrix} = \begin{bmatrix} \boldsymbol{\sigma} - \partial_{(\boldsymbol{\varepsilon}-\boldsymbol{\varepsilon}^p)} \Psi \\ \beta + \partial_\alpha \Psi \\ \chi \end{bmatrix} = \boldsymbol{0} \ . \tag{32}$$

For a general non-linear case, (32) needs to be approached using an iterative technique such as Newton-Raphson method, see also Ma et al. (2018). If the unknowns are stored in a vector $\mathscr{P} = \{\boldsymbol{\sigma}, \beta, \gamma\}$, then the linearization of $\mathscr{R}$ around the point $\mathscr{P}^i$, and the update algorithm is given by

$$\begin{aligned} \mathrm{Lin}\big[\mathscr{R}\big] &= \mathscr{R} + [\partial_{\mathscr{P}} \mathscr{R}]_{\mathscr{P}^i} \cdot [\mathscr{P}^{i+1} - \mathscr{P}^i] = \boldsymbol{0} \\ &\Longrightarrow \mathscr{P}^{i+1} = \mathscr{P}^i - \big[\partial_{\mathscr{P}} \mathscr{R}\big]^{-1} \mathscr{R}, \end{aligned} \tag{33}$$

where i denotes the local iteration index. In (33), the explicit form of the necessary iteration tangent $\partial_{\mathscr{P}} \mathscr{R}$ is given by

$$\partial_{\mathscr{P}} \mathscr{R} = \begin{bmatrix} \mathbb{I} + \gamma\, \mathbb{E} : \partial^2_{\boldsymbol{\sigma}\boldsymbol{\sigma}} \chi & \gamma\, \mathbb{E} : \partial^2_{\boldsymbol{\sigma}\beta} \chi & \mathbb{E} : \partial_{\boldsymbol{\sigma}} \chi \\ \gamma H \partial^2_{\beta\boldsymbol{\sigma}} \chi & 1 + \gamma H \partial^2_{\beta\beta} \chi & H \partial_\beta \chi \\ \partial_{\boldsymbol{\sigma}} \chi & \partial_\beta \chi & \partial_\gamma \chi \end{bmatrix} , \tag{34}$$

for the associative flow response and

$$\partial_{\mathscr{P}} \mathscr{R} = \begin{bmatrix} \mathbb{I} + \gamma\, \mathbb{E} : \partial^2_{\boldsymbol{\sigma}\boldsymbol{\sigma}} \Phi & \gamma\, \mathbb{E} : \partial^2_{\boldsymbol{\sigma}\beta} \Phi & \mathbb{E} : \partial_{\boldsymbol{\sigma}} \Phi \\ \gamma H \partial^2_{\beta\boldsymbol{\sigma}} \Phi & 1 + \gamma H \partial^2_{\beta\beta} \Phi & H \partial_\beta \Phi \\ \partial_{\boldsymbol{\sigma}} \chi & \partial_\beta \chi & \partial_\gamma \chi \end{bmatrix} , \tag{35}$$

for the non-associative flow response, along with the definitions

$$\mathbb{I} = \delta_{ik}\delta_{jl}, \quad \mathbb{E} = \partial^2_{(\boldsymbol{\varepsilon}-\boldsymbol{\varepsilon}^p)(\boldsymbol{\varepsilon}-\boldsymbol{\varepsilon}^p)} \Psi \quad \text{and} \quad H = \partial^2_{\alpha\alpha} \Psi. \tag{36}$$

The converged solution of the Newton's method (33) yields the consistent update of the vector $\mathscr{P} = \{\boldsymbol{\sigma}, \beta, \gamma\}$, which, upon insertion into (31), yields the consistent update of the set $\{\boldsymbol{\varepsilon}^p, \alpha\}$ of internal variables. The only quantity to be determined is the algorithmic elastic-plastic tangent modulus consistent with Newton's method. This can be obtained by taking the variation of the residual equations with respect to the strain. A direct calculation from (33) shows that

$$\begin{bmatrix} \boldsymbol{\sigma}^{i+1} - \boldsymbol{\sigma}^i \\ \beta^{i+1} - \beta^i \\ \gamma^{i+1} - \gamma^i \end{bmatrix} = - \begin{bmatrix} \mathscr{A}_{\boldsymbol{\sigma}\boldsymbol{\sigma}} & \mathscr{A}_{\boldsymbol{\sigma}\beta} & \mathscr{A}_{\boldsymbol{\sigma}\chi} \\ \mathscr{A}_{\beta\boldsymbol{\sigma}} & \mathscr{A}_{\beta\beta} & \mathscr{A}_{\beta\chi} \\ \mathscr{A}_{\chi\boldsymbol{\sigma}} & \mathscr{A}_{\chi\beta} & \mathscr{A}_{\chi\chi} \end{bmatrix} \begin{bmatrix} \mathscr{R}_{\boldsymbol{\sigma}} \\ \mathscr{R}_\beta \\ \mathscr{R}_\chi \end{bmatrix} , \tag{37}$$

where $\mathscr{A}_{\boldsymbol{\sigma}\boldsymbol{\sigma}}, \mathscr{A}_{\boldsymbol{\sigma}\beta}, \mathscr{A}_{\boldsymbol{\sigma}\chi}, \cdots$, are the sub-matrices of $\mathscr{A} = \big[\partial_{\mathscr{P}} \mathscr{R}\big]^{-1}$. The desired consistent tangent operator is obtained by a straightforward derivation of the first row of (37) with respect to $\boldsymbol{\varepsilon}$, taking into account (32), as

$$\mathbb{E}^{\mathrm{ep}} := \partial_{\boldsymbol{\varepsilon}} \boldsymbol{\sigma} = \partial_{\boldsymbol{\varepsilon}} (\boldsymbol{\sigma}^{i+1} - \boldsymbol{\sigma}^i) = \mathscr{A}_{\boldsymbol{\sigma}\boldsymbol{\sigma}} : \mathbb{E}. \tag{38}$$

It is noted from Eqs. (31)–(38) that, owing to the constitutive assumptions, the consistent elastic-plastic tangent modulus $\mathbb{E}^{\mathrm{ep}}$ is a fourth-order tensor that is symmetric for the associative and non-symmetric for the non-associative flow response, respectively (Miehe, 1998).

Based on (11), (20)/(24) and (30), constitutive models are implemented as user subroutines (UMAT) in (Abaqus, 2013) in three different versions for Model-I and Model-II, respectively, as

- Model-I-a/-II-a: pressure-independent model ((11) and $[(20)/(24)]|_{\eta_1 = 0}$).
- Model-I-b/-II-b: associative pressure-dependent model ((11) and (20)/(24)).
- Model-I-c/-II-c: non-associative pressure-dependent model ((11), (20)/(24) and (30)).

4. Finite element modeling and parameter calibration

The reliability of material models for a non-linear inelastic simulation not only depends on the underlying physical assumptions and accuracy of the numerical solution, but also significantly depends on the accurate deduction of the material parameters from the experimental data. This scenario, referred to as the inverse problem of *parameter identification*, involves the search of optimal parameters for a given material model, boundary conditions, the resulting simulated material response and the available experimental data. Mathematically, the parameter identification problem represents a *non-linear optimization* problem subject to inequality constraints, where the constraints are due to the physical restrictions on the values that the material parameters may attain. The solution of this problem relies on methods of non-linear optimization described in the literature (Press et al., 1992; Yun and Shang, 2011; Li et al., 2016).

In this section, aspects of finite element implementation and the parameter calibration procedure for the homogenized models developed in Section 2, are described in detail. While the elastic parameters are taken directly from Vogler and Kyriakides (1999) and Hsu et al. (1999), the parameters describing the plastic response, i.e. y_{12}, y_{23}, y_{22c}, h and n in (11) and (20)/(24), are calibrated by an optimization procedure. To this end, parameters y_{12}, h and n are calibrated from the non-linear in-plane shear stress-strain curve, y_{23} is calibrated from the transverse shear stress-strain curve and y_{22c} is calibrated from the transverse compression data. The experimental data for the present study is taken from Vogler and Kyriakides (1999) and Hsu et al. (1999), which provides the in-plane shear stress curve (Fig. 3(a) from Hsu et al. (1999)) and the transverse compression curve (Fig. 4(b) at $\dot{\varepsilon}_0 = 1.5 \times 10^{-4}$ from Hsu et al. (1999)). Due to the lack of experimental data for the transverse shear (23-) response, *micromechanical* models are used to generate missing data from the procedure described next.

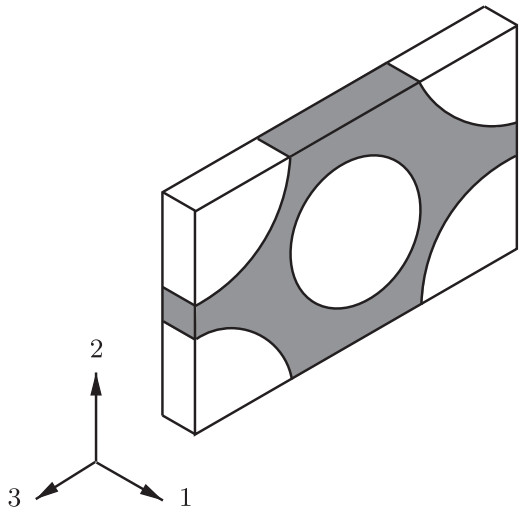

Fig. 1. Finite element models. Geometrical setup of the unit cell (UCA).

4.1. Finite element models

For the parameter calibration and verification of the material models, finite element models are analyzed with ABAQUS. In addition to the homogenized models, two types of micromechanical models are used in the present study, a unit cell analysis (UCA) with hexagonal arrangement, see Fig. 1 (with hexagonal arrangement being used rather than a square arrangement since it is a better representation of reality according to Hsu et al. (1999)), and an incremental Mori-Tanaka approach using DIGIMAT (DIG) (DIGIMAT, 2018). For a detailed discussion on the incremental Mori-Tanaka approach cf. to Pettermann et al. (1993), Doghri and Ouaar (2003), Doghri et al. (2010). For both micromechanical models, fibers are assumed to be linear elastic and transversely isotropic with a fiber volume fraction of 60%. The matrix is assumed to be an isotropic elastic-plastic solid with rate and pressure-independent plasticity using power law hardening. Due to availability in the software packages, slightly different formulations are used; a standard J_2-plasticity in the case of the DIGIMAT model (DIGIMAT, 2018) and the *Johnson-Cook* material model provided by ABAQUS for the UCA (Abaqus, 2013). Johnson-Cook hardening is a particular type of isotropic hardening where the yield stress σ_y is of the form

$$\sigma_y = A + B(\bar{\varepsilon}^{pl})^n \tag{39}$$

where $\bar{\varepsilon}^{pl}$ is the equivalent plastic strain, and A, B and n are the plastic material parameters. The elastic properties of fibers and the matrix are given in (Hsu et al., 1999) and stated in Table 1, whereas the plastic parameters are calibrated from the experimental data based on the $\tau_{12} - \gamma_{12}$ curve using the calibration procedure defined below.

All the finite element models use periodic boundary conditions and are discretized using hexahedral 3D continuum elements (C3D8) with linear interpolation. For the UCA, the unit cell is discretized into 122 C3D8 elements. A convergence study of UCA showed no change of the overall stress-strain response with higher mesh refinement. For the simulations of the DIG and the homogenized models, a single C3D8 element is used.

4.2. Calibration procedure

The plastic parameters of all models are obtained with the same general procedure, where parameters are calculated by a least squares minimization of the function

$$f(\boldsymbol{x}) = \frac{1}{k}\sum_{k=1}^{n} \left\| \bar{\boldsymbol{\delta}}_k - \boldsymbol{\delta}_k(\boldsymbol{x}) \right\| \rightarrow \min . \tag{40}$$

Here, $\bar{\boldsymbol{\delta}}_k$ and $\boldsymbol{\delta}_k(\boldsymbol{x})$ represent target and computed values respectively and $k = 1, \cdots, n$ are the identification points at which target and computed values are to be compared. $\boldsymbol{x}$ is an array of fitting parameters, i.e. $\boldsymbol{x} = \{A, B, n\}$ for micromechanical models calibration, $\boldsymbol{x} = \{y_{12}, h, n\}$ and $\boldsymbol{x} = \{y_{23}\}$ for Model-I-a/-II-a calibration and $\boldsymbol{x} = \{y_{22c}\}$ for Model-I-b/-II-b as well as Model-I-c/-II-c calibration. A simplex Nelder–Mead algorithm (Press et al., 1992; Mahnken et al., 2009) is used for the minimization of Eq. (40).

For the micromechanical models, only the in-plane shear curve is needed to calibrate the parameters for matrix plasticity A, B and n (since pressure dependency is not considered in these models). With the calibrated micromechanical models, $\sigma_{22} - \varepsilon_{22}$ and $\tau_{23} - \gamma_{23}$ responses can be computed. It should be noted, that on the micro level under 23-shear loading, only phase averaged stresses show zero hydrostatic pressure. Due to stress concentrations in the matrix, the UCA model locally shows a hydrostatic component which may affect the overall plasticity response. It has been found that this effect is rather low compared to variations caused by e.g. fiber arrangement and is therefore neglected. The transverse compression curve, which also does not include pressure sensitivity of the matrix is not used for calibration but instead is used as an additional verification of the meso-scopic pressure-independent models, Model-I-a and Model-II-a. By considering pressure-independent models under transverse compression it is possible to distinguish between effects of anisotropicity (due to the micro structure) and pressure dependency of the matrix - a distinction that can not be inferred from experimental data. Similarly, to calibrate the plastic parameters of the homogenized models, the calibration procedure is first used to obtain y_{12}, h and n of Model-I-a/-II-a by fitting to the experimental data of the in-plane shear response. Keeping these parameters fixed, y_{23} values for Model-I-a and Model-II-a are obtained from the curves of the calibrated micromechanical models. Finally, y_{22c} values for the pressure-dependent models Model-I-b/-II-b and Model-I-c/-II-c are obtained from the experimental $\sigma_{22} - \varepsilon_{22}$ curve. The calibrated plastic parameters for all the models are summarized in Tables 1 and 2.

Table 1
Material parameters for the micromechanical models.

No.	Name	Par.	Value	Unit
			DIG/UCA	
	Fiber			
1.	Longitudinal young's modulus	E_{1f}	214,000	[MPa]
2.	Transverse young's modulus	E_{2f}	26,000	[MPa]
3.	Longitudinal shear modulus	G_{12f}	112,000	[MPa]
4.	Transverse shear modulus	G_{23f}	8996.3	[MPa]
5.	Poisson's ratio	ν_{12f}	0.28	[-]
	Matrix			
6.	Young's modulus	E_m	4100	[MPa]
7.	Poisson's ratio	ν_m	0.356	[-]
8.	Initial yield stress	A	13.05/12.99	[MPa]
9.	Hardening modulus	B	187/220.05	[MPa]
10.	Hardening exponent	n	0.269/0.228	[-]

4.3. Calibration results

Results of the calibration comparing the experimental data and various models for the three calibration load cases are shown in Fig. 2. It is evident that all the constitutive models can be fit-

Table 2
Material parameters for the homogenized models.

No.	Name	Par.	Value	Unit
			Model-I/Model-II	
1.	Longitudinal young's modulus	E_1	130000	[MPa]
2.	Transverse young's modulus	E_2	11000	[MPa]
3.	Longitudinal shear modulus	G_{12}	5800	[MPa]
4.	Transverse shear modulus	G_{23}	3720	[MPa]
5.	Poisson's ratio	ν_{12}	0.306	[–]
6.	Transverse compressive yield stress	y_{22c}	$\begin{cases} 45.9/24.6^a \\ 50.01/27.4^b \end{cases}$	[MPa]
7.	In-plane shear yield stress	y_{12}	17.9/9.41	[MPa]
8.	Transverse shear yield stress	y_{23}	15.9/10.66	[MPa]
9.	Hardening modulus	h	192.3/177.5	[MPa]
10.	Pre-strain	$\bar{\alpha}$	10^{-12}	[–]
11.	Hardening exponent	n	0.296/0.246	[–]

[a]Model-I-b/-II-b
[b]Model-I-c/-II-c

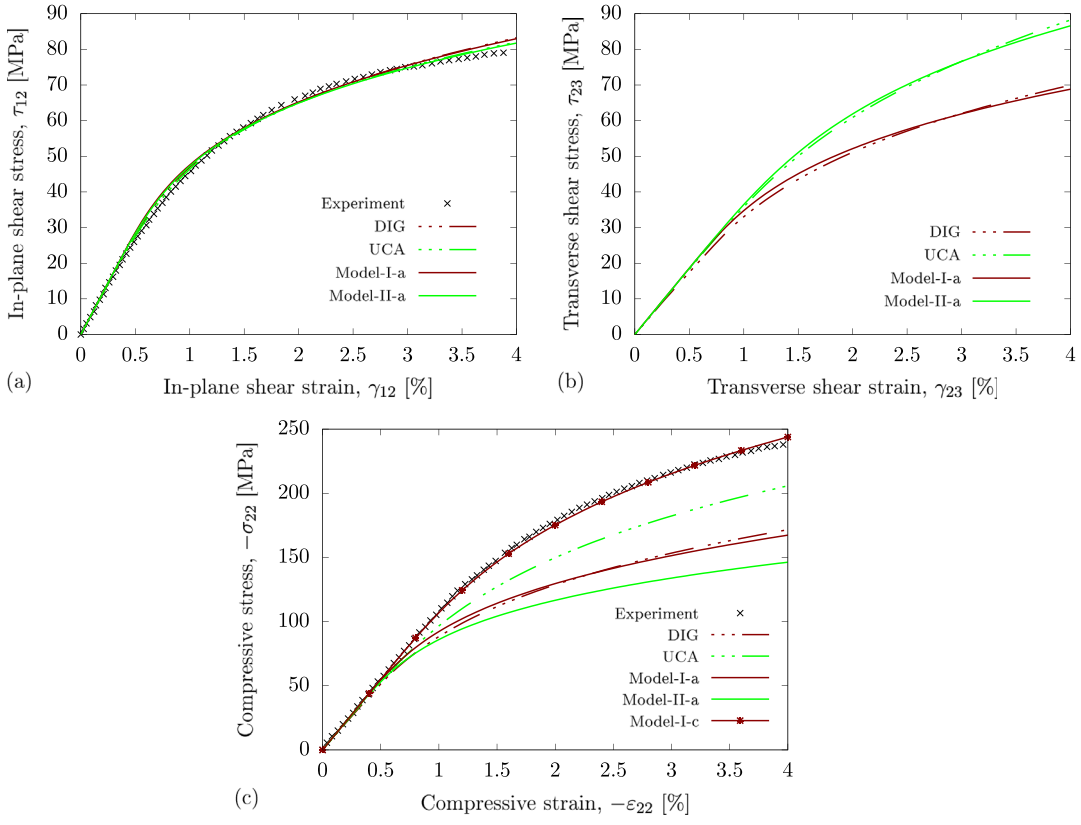

Fig. 2. Calibration results. Comparison of experimental, micromechanical and homogenized models responses for (a) in-plane shear, (b) transverse shear and (c) transverse compression load.

ted to the experimental shear ($\tau_{12} - \gamma_{12}$) curve very well using the power law. Further, the numerical results in Fig. 2(a) and (b) show that the transverse shear response is stiffer than the in-plane shear response for UCA, whereas the transverse shear response is softer than the in-plane shear response for DIG. The main reason for the difference between the two predictions is the fact that mean field methods such as the incremental Mori-Tanaka approach used by DIG are based on analytical solution of phase averaged stresses that do not take stress concentrations and details of the fiber arrangement into account. As a result, such incremental Mori-Tanaka schemes are less accurate than discrete unit-cell predictions. As mentioned in Section 2.3.1 and given by Eq. (A.9) of Appendix A, this readily implies that the convexity requirement for Model-I is not fulfilled for calibration to UCA.

Hence, Model-I is calibrated to DIG and Model-II is calibrated to UCA. Note that calibrating y_{23} for Model-II to DIG would be admissible as well, however this comparison does not yield any additional qualitative insights and is therefore not discussed further in this work.

Fig. 2(c) shows the comparison of micromechanical and homogenized models to the experimental response for a transverse compression load. It can be seen that the compressive response of Model-I-a fits the DIG model very well whereas Model-II-a is significantly less stiff than UCA in the non-linear compression regime. As stated and computationally verified in (Hsu et al., 1999), this behavior can be corrected by taking into account the influence of hydrostatic pressure in the formulation of plastic response functions. Therefore, Model-I-b/-II-b and Model-I-c/-II-c are used to capture the experimental transverse compression ($\sigma_{22} - \varepsilon_{22}$) data by calibrating y_{22c}. The resulting good agreement between the experimental data and Model-I-c is shown in Fig. 2(c). Analogously, Model-I-b/-II-b and Model-II-c can be calibrated for y_{22c} to give basically the same compressive response as Model-I-c. It should be noted, however, that in order to fit the compression test curve, Model-II requires more pressure sensitivity than Model-I. Furthermore, y_{22c} values also differ slightly between associative (b) and non-associative (c) models.

5. Models evaluation

The constitutive homogenized models defined and calibrated in Sections 2–4 are first verified for the correctness of the implementation. Next, the predictions of the calibrated homogenized models are compared to those of the micromechanical models and experiments for a range of bi-axial load cases given in (Vogler and Kyriakides, 1999). The material parameters used for the simulations are given in Tables 1 and 2.

5.1. Effect of pressure dependency

To demonstrate the effect of hydrostatic pressure, the six constitutive models summarized in Section 3 are subjected to two test cases. Note that for comparison purposes, in this section, the same transverse compressive yield stresses are used for associative and non-associative pressure-dependent models, i.e. $y_{22c} = 50.32$ MPa for Model-I-b/-I-c and $y_{22c} = 27.97$ MPa for Model-II-b/-II-c, such that differences in the predicted response can be purely attributed to differences in the model formulations.

The first test case is a uni-axial transverse tension and compression test up to a strain magnitude of $\varepsilon_{22} = \pm 4\%$, the results of which are shown in Fig. 3(a) for Model-I and Fig. 3(c) for Model-II. As expected, the pressure-independent model behaves symmetrically in the tension and compression regime. In contrast, the two pressure-dependent models exhibit the well-known tension-compression asymmetry where the difference between the yield limits in the tension and the compression load is observed. Also, the tensile response is softer than the compressive response.

As a second example, a combined compression-shear test is analyzed where a full shear loading cycle is superimposed by additional transverse strain such that pressure dependency leads to a distinction between the different model versions. To this end, a compressive strain of magnitude $\varepsilon_{22} = -1.5\%$ is first applied. While ε_{22} is kept fixed, the specimen is sheared up to a shear strain of $\gamma_{12} = +4\%$, then unloaded and reloaded in the opposite direction up to $\gamma_{12} = -4\%$, and finally again reloaded to $\gamma_{12} = +4\%$. The computed results for one shear cycle are shown

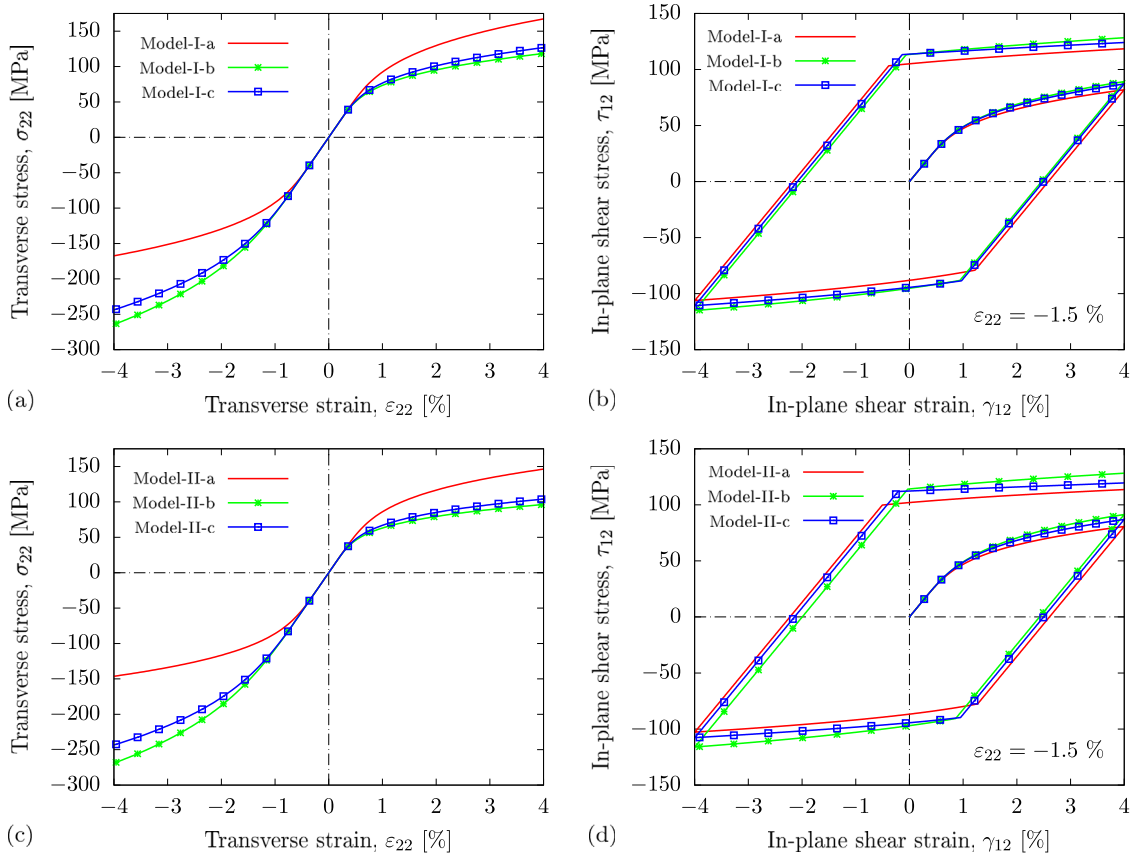

Fig. 3. Effect of pressure dependency. Stress-strain curves of a single element test for (a), (c) transverse load and (b), (d) in-plane shear with pre-compression load of Model-I and Model-II, respectively.

Table 3
Summary of the radial load paths.

Load path No.	τ_{12}^f (MPa)	$-\sigma_{22}^f$ (MPa)	$\lambda = -\sigma_{22}^f/\tau_{12}^f$ (-)
⑭	79.50	0	0
⑩	30.07	215.6	7.17
⑪	65.34	192.1	2.94
⑫	84.03	164.7	1.96
⑬	92.85	91.0	0.98

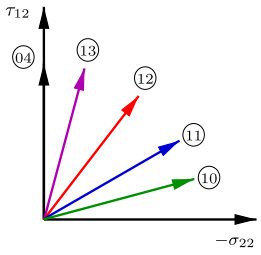

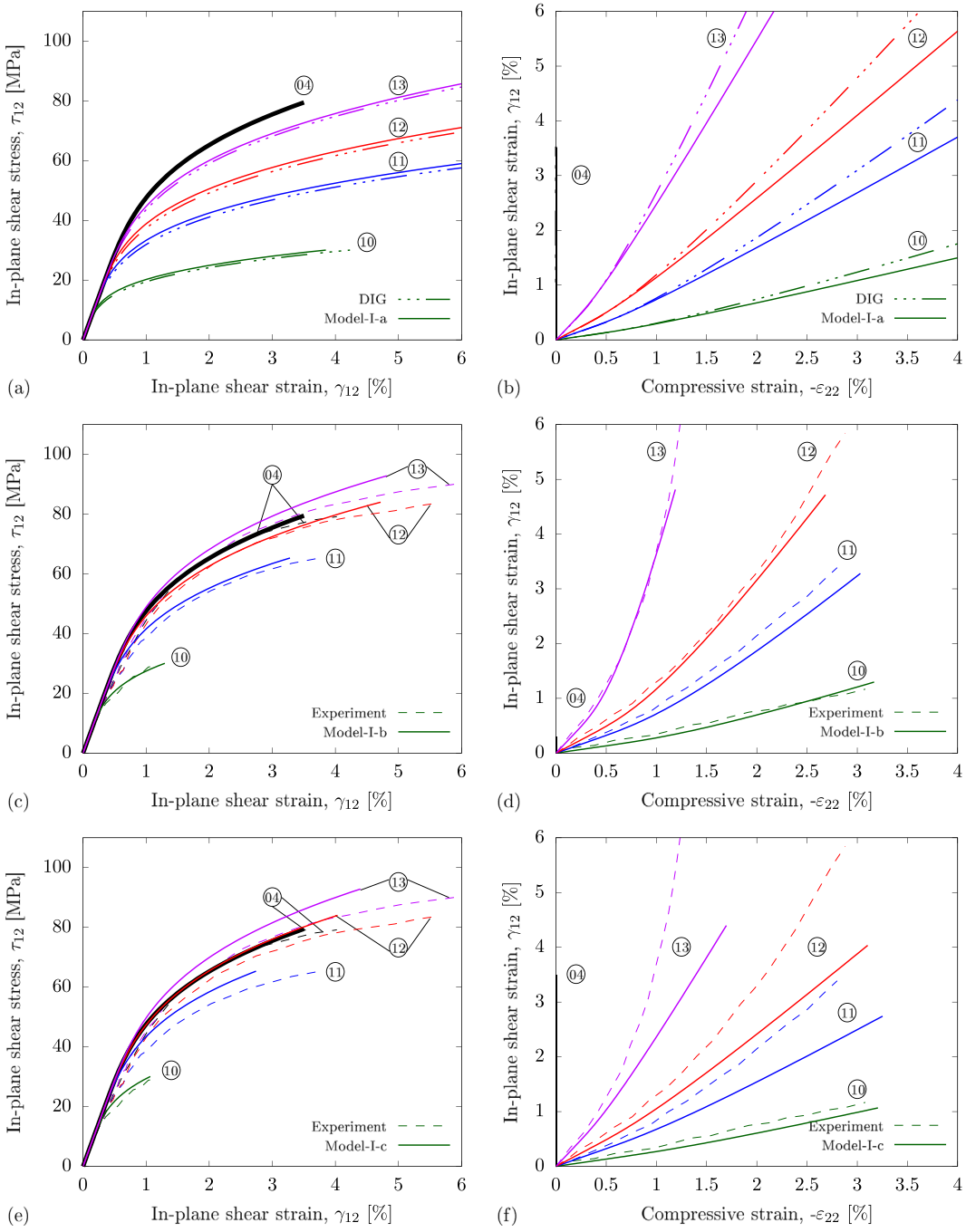

Fig. 4. Quantitative evaluation. Comparison of (a), (b) DIG and Model-I-a; (c), (d) experimental and Model-I-b and (e), (f) experimental and Model-I-c responses for various proportionality factors of the radial load case.

in Fig. 3(b) for Model-I and Fig. 3(d) for Model-II. The figures nicely show the effect of the isotropic hardening formulation. Furthermore, it can be observed that the pressure-independent models show the highest amount of plasticity leading to a slightly lower tangent stiffness during plastic deformation than the other models. During unloading, the elastic stiffness is recovered until the yielding is again reached, followed by further plastic deformation with the same tangent stiffness at the beginning. Since the hardening parameters are identical for the pressure-independent and the pressure-dependent models, it is expected that the predicted response of the non-associative pressure-dependent model is bounded by the pressure-independent model and the associative pressure-dependent model. The numerical results in Fig. 3(a)–(d) are in agreement with this prediction. These results are similar to the observations of Mosler and Bruhns (2009) in their work on finite strain plasticity.

5.2. Quantitative evaluation of plasticity models.

The predictions of Model-I and Model-II are now compared to those of DIG and UCA as well as experimental results from the literature (Vogler and Kyriakides, 1999) for a set of load paths with proportional increase of compressive and shear stresses. Four different proportionality factors, $\lambda = -\sigma_{22}^f/\tau_{12}^f$, given in (Vogler and Kyriakides, 1999), are considered which are summarized in Table 3. For the numerical investigations, simulations are loaded up to fi-

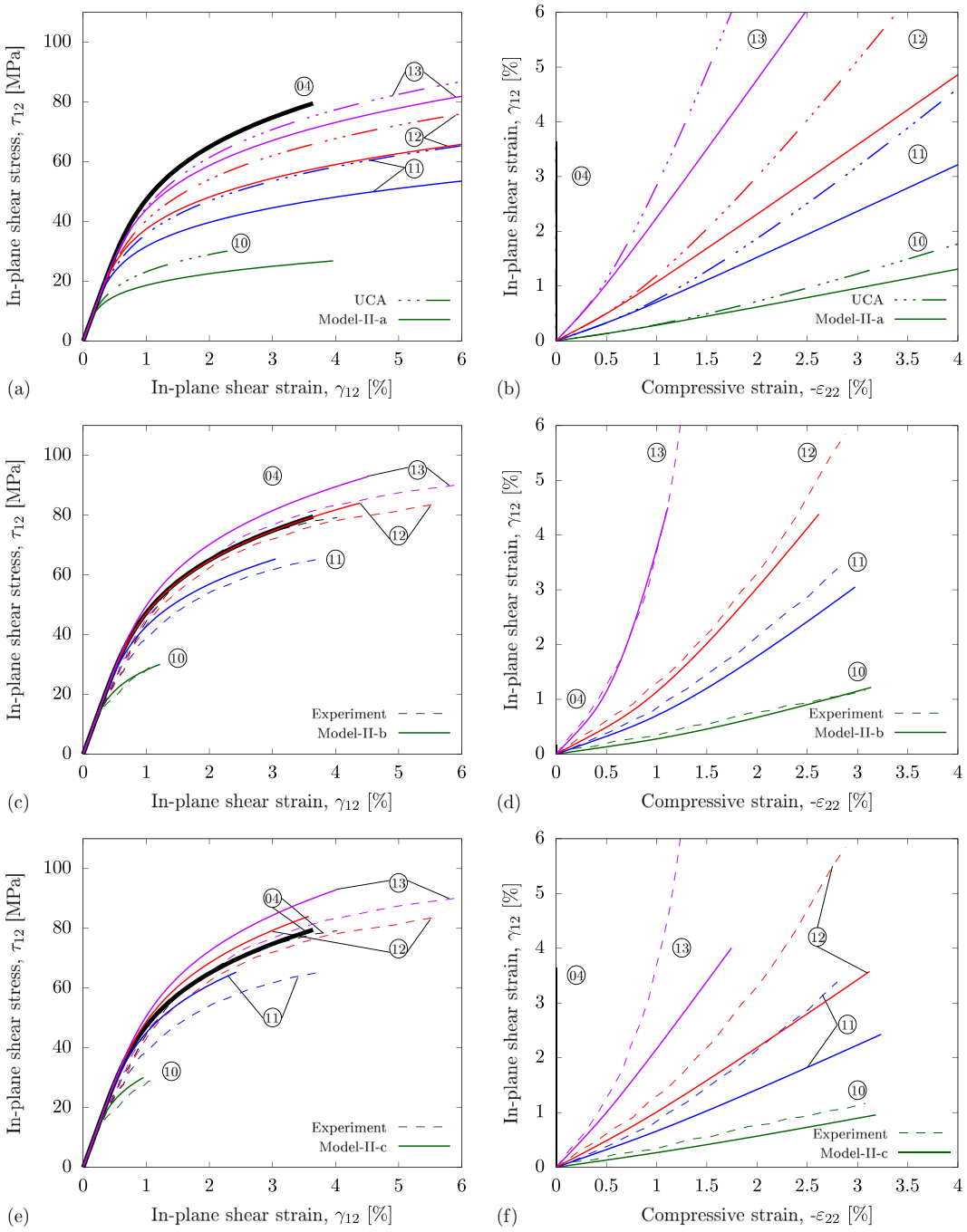

Fig. 5. Quantitative evaluation. Comparison of (a), (b) UCA and Model-II-a; (c), (d) experimental and Model-II-b and (e), (f) experimental and Model-II-c responses for various proportionality factors of the radial load case.

nal stress values from the experiments (also listed in Table 3). Plots depicting Model-I and Model-II predictions are shown in Figs. 4 and 5, respectively. Figs. 4(a) & (b) and 5(a) & (b) compare micromechanical and pressure-independent homogenized models, i.e. DIG vs. Model-I-a and UCA vs. Model-II-a (see in this context Section 4.3). The response predicted by Model-I-a is in very good agreement with that of DIG, whereas Model-II-a shows a softer response than UCA for higher proportionality factors λ, similar to what is observed in calibration (see Fig. 2). Figs. 4(c)–(f) and 5(c)–(f) show the comparison of pressure-dependent models to the experimental response from Vogler and Kyriakides (1999), Hsu et al. (1999). The assessment of pressure dependency can best be observed in Figs. 4(c) & (e) and 5(c) & (e). In contrast to pressure-independent models (Figs. 4(a) and 5(a)), where curves shift down with increasing λ, the experimental results show that the stress-strain response first shifts up (from to ⑬) before shifting down again. This general behavior is captured by Model-I-b/-II-b and Model-I-c/-II-c, which shows that pressure dependency is needed in order to recover the behavior observed experimentally. The shear response of the load path ⑩ is captured quite well by all models. Predictions for the load path ⑬ shows that there is slightly too much pressure sensitivity in all models with best fit for Model-I-b and worst fit Model-II-c.

It is interesting to note that the micro-model proposed by Hsu et al. (1999) captures this influence of additional transverse compression on the in-plane shear response (i.e. the upward shifting from curve to ⑬) without the need of pressure dependency (see Fig. 9 in (Hsu et al., 1999)). This is also the reason why adding pressure sensitivity in the Hsu-model leads to an overly stiff shear response for biaxial load cases (i.e. curves ⑩ – ⑬, see Fig. 12 in (Hsu et al., 1999)), while in our models, adding pressure dependency improves correlation for both in-plane shear and transverse compressive behavior under biaxial loads.

The assessment of plastic flow direction is apparent in strain plots γ_{12} vs. $-\varepsilon_{22}$ of Figs. 4 and 5. Model-I-a agrees fairly well with DIG, whereas with Model-II-a, almost a linear relation between the shear and compressive behavior is seen. Furthermore, the associative pressure-dependent model seems to work better than the non-associative counterpart. An argument in (Hsu et al., 1999) suggests that the non-associative model is better than the associative model because of change in the curvature for non-radial loads, a behavior also observed in our case but only for a very low amount of preload. The direction of plastic flow is generally captured better by the micro-models proposed by Hsu et al. (1999) (especially Model I). In our meso-models, this depends on the slope of pressure dependency, which should be rather low based on the experimental shear response of the load paths and ⑬, wherefore, the associative pressure-dependent model reproduces the experimentally observed behavior more accurately for the test data considered. Plastic dilation can be observed in polymers due to crazing (Chen et al., 2016; Zaïri et al., 2008), however, it is unknown if crazing was observed in the tests considered here.

6. Conclusions

This articles develops two new relatively general mesomodels for the nonlinear, elastic-plastic response of polymer composites reinforced by UD fibers. Two forms of plastic response functions (Model-I and Model-II) formulated in terms of a plasticity inducing stress tensor, are proposed. From a theoretical standpoint, Model-I cannot be used in situations where the transverse shear response is stiffer than the in-plane shear response, as per the convexity requirement. This constraint is not applicable to Model-II. From a computational standpoint, the use of plasticity inducing stress in the formulation of plastic response functions results in the decoupled representation of the shear terms thus simplifying the problem of parameter identification.

All the constitutive models are first calibrated to reproduce the experimental pure shear response. The pressure-independent models capture the experimental shear response quite well, however, the compressive response predicted is observably less stiff. The associative and the non-associative versions of the pressure-dependent models calibrated in a similar manner are found to overcome this deficiency, as suggested and computationally verified in (Hsu et al., 1999).

The calibrated homogenized models are evaluated in detail by comparison to micromechanics simulations and experimental data for a range of bi-axial loads. Overall, the constitutive models perform well in predicting the trends of the observed behavior. Though the pressure-dependent models predict the compressive response accurately, the shear response in presence of compression is slightly overpredicted for some load paths, mostly by the non-associative pressure-dependent models. Also, in the non-associative case, there is an observable deviation between the bi-axial experimental response and the model predicitions. This can purely be attributed to the respective models formulation, where it has been assumed that the plastic flow is deviatoric and stress free in the fiber direction. In view of these characteristics, it is currently being investigated if dilatancy is observed during the plastic deformation, i.e. the plastic flow potential is formulated such that it is pressure dependent but stress free in the fiber direction. To the authors knowledge, this modification gives better results than the presented non-associative models. Further issues regarding the elastic-plastic behavior of composite materials such as the effect of fibers on plasticity for a combination of shear/compressive load with tension/compression in the fiber direction, kinematic hardening effects and rate-dependent plastic behavior are also being pursued.

Acknowledgments

SGN gratefully acknowledges fruitful and stimulating discussions with Professor Thomas Antretter from the Institute of Mechanics at MU Leoben. The authors would also like to thank Associate Professors Helmut J. Böhm and Heinz Pettermann from the Institute of Lightweight Design and Structural Biomechanics at TU Vienna for their interest and helpful comments.

Appendix A. Convexity of the yield surface: Model-I

In this appendix, the proof of convexity of the yield surface for Model-I is shown. For the particular model at hand, recall the yield function

$$\chi = \eta_1 \tilde{J}_1 + \left[\eta_2 \tilde{J}_2 + \eta_3 \tilde{J}_3\right]^{1/2} - \left(1 - \frac{\beta}{y_{12}}\right) \leq 0. \tag{A.1}$$

Mathematically, the convexity of the yield surface χ is demonstrated if it can be shown that the Hessian matrix $\mathbb{Z}$ of this function is positive semi-definite, i.e. its eigenvalues are all positive or zero, see Voyiadjis and Thiagarajan (1995). The Hessian matrix for the function (A.1) is defined as,

$$\mathbb{Z} = \partial^2_{\boldsymbol{\sigma}\boldsymbol{\sigma}} \chi = \frac{\eta_3 \mathbb{P} + (\eta_2 - \eta_3)\mathbb{P}_a}{\left[\eta_2 \tilde{J}_2 + \eta_3 \tilde{J}_3\right]^{1/2}} - \frac{\eta_3^2 \mathbb{J} + \eta_3(\eta_2 - \eta_3)\{\mathbb{K} + \mathbb{L}\} + (\eta_2 - \eta_3)^2 \mathbb{M}}{\left[\eta_2 \tilde{J}_2 + \eta_3 \tilde{J}_3\right]^{3/2}} \tag{A.2}$$

along with the definitions

$$\begin{aligned}\mathbb{P} &= \mathbb{I} - \frac{1}{3}(\boldsymbol{1}\otimes\boldsymbol{1}) - \frac{3}{2}(\boldsymbol{m}'\otimes\boldsymbol{m}')\\ \mathbb{P}_a &= \boldsymbol{m}\mathbb{P} + \mathbb{P}\boldsymbol{m}\\ \mathbb{J} &= \boldsymbol{s}\otimes\boldsymbol{s}\\ \mathbb{K} &= \boldsymbol{s}\otimes\{\boldsymbol{m}\boldsymbol{s}+\boldsymbol{s}\boldsymbol{m}\}\\ \mathbb{L} &= \{\boldsymbol{m}\boldsymbol{s}+\boldsymbol{s}\boldsymbol{m}\}\otimes\boldsymbol{s}\\ \mathbb{M} &= \{\boldsymbol{m}\boldsymbol{s}+\boldsymbol{s}\boldsymbol{m}\}\otimes\{\boldsymbol{m}\boldsymbol{s}+\boldsymbol{s}\boldsymbol{m}\},\end{aligned} \tag{A.3}$$

where $\boldsymbol{s}$ is the second-order plasticity inducing stress tensor defined in (16). Furthermore, the set of eigenvalues of (A.2) in terms of the stress components are given by

$$\lambda_{\mathbb{Z}} = \left\{0, 0, 0, \frac{\eta_2}{\sqrt{2}\sqrt{4\eta_2(\sigma_{12}^2+\sigma_{13}^2)+4\eta_3\sigma_{23}^2+\eta_3(\sigma_{22}-\sigma_{33})^2}}, \frac{4\eta_2\eta_3(3\sigma_{12}^2+3\sigma_{13}^2+\sigma_{23}^2)+\eta_3(\eta_2+\eta_3)(\sigma_{22}-\sigma_{33})^2+8\eta_3^2\sigma_{23}^2-\Im}{2\sqrt{2}\left(\sqrt{4\eta_2(\sigma_{12}^2+\sigma_{13}^2)+4\eta_3\sigma_{23}^2+\eta_3(\sigma_{22}-\sigma_{33})^2}\right)^3}, \frac{4\eta_2\eta_3(3\sigma_{12}^2+3\sigma_{13}^2+\sigma_{23}^2)+\eta_3(\eta_2+\eta_3)(\sigma_{22}-\sigma_{33})^2+8\eta_3^2\sigma_{23}^2+\Im}{2\sqrt{2}\left(\sqrt{4\eta_2(\sigma_{12}^2+\sigma_{13}^2)+4\eta_3\sigma_{23}^2+\eta_3(\sigma_{22}-\sigma_{33})^2}\right)^3}\right\}, \tag{A.4}$$

with

$$\begin{aligned}\Im = \Big\{&\big[4\eta_2\eta_3(\sigma_{12}^2+\sigma_{13}^2-\sigma_{23}^2)\\ &+\eta_3(\eta_2-\eta_3)(\sigma_{22}-\sigma_{33})^2+8\eta_3^2\sigma_{23}^2\big]^2\\ &+16\eta_3^2\sigma_{23}^2(\sigma_{22}-\sigma_{33})^2\big[2\eta_3^2-3\eta_2\eta_3+\eta_2^2\big]\Big\}^{1/2}.\end{aligned} \tag{A.5}$$

The only condition that is mathematically imposed on η_2 and η_3 is that they both must be greater than zero, since they are magnitudes of yield strengths. This condition is also physically satisfied in their computation, as seen in (21). Therefore, without any restrictions, it can be assumed that $\eta_{2,3} > 0$. From (A.4) it is directly seen that $\lambda_{\mathbb{Z}(1)}$, $\lambda_{\mathbb{Z}(2)}$, $\lambda_{\mathbb{Z}(3)}$ and $\lambda_{\mathbb{Z}(4)}$ are all ≥ 0. For $\lambda_{\mathbb{Z}(5)}$ to be ≥ 0, the following condition should be true

$$\frac{4\eta_2\eta_3(3\sigma_{12}^2+3\sigma_{13}^2+\sigma_{23}^2)+\eta_3(\eta_2+\eta_3)(\sigma_{22}-\sigma_{33})^2+8\eta_3^2\sigma_{23}^2}{2\sqrt{2}\left(\sqrt{4\eta_2(\sigma_{12}^2+\sigma_{13}^2)+4\eta_3\sigma_{23}^2+\eta_3(\sigma_{22}-\sigma_{33})^2}\right)^3} \geq \frac{\Im}{2\sqrt{2}\left(\sqrt{4\eta_2(\sigma_{12}^2+\sigma_{13}^2)+4\eta_3\sigma_{23}^2+\eta_3(\sigma_{22}-\sigma_{33})^2}\right)^3}. \tag{A.6}$$

Rearranging the expression by squaring both sides yields

$$\begin{aligned}&\big[4\eta_2\eta_3(3\sigma_{12}^2+3\sigma_{13}^2+\sigma_{23}^2)+\eta_3(\eta_2+\eta_3)(\sigma_{22}-\sigma_{33})^2+8\eta_3^2\sigma_{23}^2\big]^2 \geq\\ &\big[4\eta_2\eta_3(\sigma_{12}^2+\sigma_{13}^2-\sigma_{23}^2)+\eta_3(\eta_2-\eta_3)(\sigma_{22}-\sigma_{33})^2+8\eta_3^2\sigma_{23}^2\big]^2\\ &+16\eta_3^2\sigma_{23}^2(\sigma_{22}-\sigma_{33})^2\big[2\eta_3^2-3\eta_2\eta_3+\eta_2^2\big]\end{aligned} \tag{A.7}$$

After expanding (A.7) and canceling out similar terms, it is observed that the quantity on the LHS is positive where as that on the RHS is negative, implying $\lambda_{\mathbb{Z}(5)}$ is ≥ 0. For $\lambda_{\mathbb{Z}(6)}$ to be ≥ 0, it needs to be shown that

$$\frac{\Im}{2\sqrt{2}\left(\sqrt{4\eta_2(\sigma_{12}^2+\sigma_{13}^2)+4\eta_3\sigma_{23}^2+\eta_3(\sigma_{22}-\sigma_{33})^2}\right)^3} \geq 0 \tag{A.8}$$

which is a priori true for

$$\begin{aligned}&16\eta_3^2\sigma_{23}^2(\sigma_{22}-\sigma_{33})^2\big[2\eta_3^2-3\eta_2\eta_3+\eta_2^2\big] \geq 0\\ &\Rightarrow \eta_3 \geq \eta_2 \Rightarrow y_{12} \geq y_{23}.\end{aligned} \tag{A.9}$$

The above inequality is the necessary condition for the yield surface to be convex in the stress space.

References

Abaqus, 2013. ABAQUS/Standard User's Manual, Version 6.13-2. Dassault Systemés Simulia Corp., Providence, RI, USA.

Al-Haik, M., Garmestani, H., Savran, A., 2004. Explicit and implicit viscoplastic models for polymeric composite. Int. J. Plast. 20 (10), 1875–1907.

Aldakheel, F., Miehe, C., 2017. Coupled thermomechanical response of gradient plasticity. Int. J. Plast. 91, 1–24.

Boehler, J., 1979. A simple derivation of representations for non-polynomial constitutive equations in some case of anisotropy. ZAMM 59, 157–167.

Car, E., Oller, S., Oñate, E., 2000. An anisotropic elastoplastic constitutive model for large strain analysis of fiber reinforced composite materials. Comput. Methods Appl. Mecha.Eng. 185, 245–277.

Car, E., Oller, S., Oñate, E., 2001. A large strain plasticity model for anisotropic materials-composite material application. Int. J. Plast. 17, 1437–1463.

Casey, J., 1984. A simple proof of a result in finite plasticity. Q. Appl. Math. 42, 61–71.

Chaboche, J., 2008. A review of some plasticity and viscoplasticity constitutive theories. Int. J. Plast. 24, 1642–1693.

Chang, F., Chang, K.-Y., 1987. A progressive damage model for laminated composites containing stress concentrations. J. Compos. Mater. 21(9), 834–855.

Chen, F., Gatea, S., Ou, H., Lu, B., Long, H., 2016. Fracture characteristics of PEEK at various stress triaxialities. J. Mech. Behav. Biomed.Mater. 64, 173–186.

Chen, J., Sun, C., 1993. A plastic potential function suitable for anisotropic fiber composites. J. Compos. Mater. 27, 1379–1390.

Colak, O., 2005. Modeling deformation behavior of polymers with viscoplasticity theory based on overstress. Int. J. Plast. 21 (1), 145–160.

Cordoso, R., Adetoro, O., 2017. A generalisation of the Hill's quadratic yield function for planar plastic anisotropy to consider loading direction. Int. J. Mech. Sci. 128–129, 253–268.

DIGIMAT User's Manual. 2018. e-Xstream engineering, MSC Software Corporation.

Doghri, I., Adam, L., Bilger, N., 2010. Mean-field homogenization of elasto-viscoplastic composites based on a general incrementally affine linearization method. Int. J. Plast. 26 (2), 219–238.

Doghri, I., Ouaar, A., 2003. Homogenization of two-phase elasto-plastic composite materials and structures. study of tangent operators, cyclic plasticity and numerical algorithms. Int. J. Solids Struct. 40, 1681–1712.

Drucker, D., 1964. On the postulate of stability of materials in mechanics of continua. J. Mécanique 3, 235–249.

Dvorak, G., Bahei-El-Din, Y., 1987. A bimodal plasticity theory of fibrous composite materials. Acta Mechanica 69, 219–241.

Dvorak, G., Bahei-El-Din, Y., Macharet, Y., Liu, C., 1988. An experimental study of elastic-plastic behavior of a fibrous boron-aluminum composite. J. Mech. Phys. Solids 36, 655–687.

Flatscher, T., Schuecker, C., Pettermann, H., 2013. A constitutive ply model for stiffness degradation and plastic strain accumulation: its application to the third world wide failure exercise (part a). J. Compos. Mater. 47, 2575–2593.

Gilat, A., Goldberg, R., Roberts, G., 2005. Strain Rate Sensitivity of Epoxy Resin in Tensile and Shear Loading. Technical Report, TM-2005-213595.

G'sell, C., Jacques, D., Favre, J., 1990. Plastic behavior under simple shear of thermosetting resins for fiber composite matrices. J. Mater. Sci. 25, 2004–2010.

Hill, R., 1950. The mathematical Theory of Plasticity. Oxford: Clarendon Press.

Hsu, S.-Y., Vogler, T., Kyriakides, S., 1999. Inelastic behavior of an AS4/PEEK composite under combined transverse compression and shear. Part II: modeling. Int. J. Plast. 15, 807–836.

Kontou, E., Spathis, G., 2006. Application of finite strain viscoplasticity to polymeric fiber composites. Int. J. Plast. 22 (7), 1287–1303.

Lemaitre, J., 1992. A Course on Damage Mechanics. Springer-Verlag, Berlin, Heidelberg, Germany.

Li, H., Hu, X., Yang, H., Li, L., 2016. Anisotropic and asymmetrical yielding and its distorted evolution: modeling and applications. Int. J. Plast. 82, 127–158.

Liu, I.-S., 1982. On representations of anisotropic invariants. Int. J. Eng. Sci. 31, 1099–1109.

Lu, J., Zhang, L., 2005. Physically motivated invariant formulation for transversely isotropic hyperelasticity. Int. J. Solids Struct. 42, 6015–6031.

Lubliner, J., 1997. Plasticity Theory. Maxwell Macmillan International Edition.

Ma, R., Pilchak, A., Semiatin, S., Truster, T., 2018. Modeling the evolution of microtextured regions during α/β processing using the crystal plasticity finite element method. Int. J. Plast. 107, 189–206.

Mahnken, R., Schneidt, A., Antretter, T., 2009. Macro modelling and homogenization for transformation induced plasticity of a low alloy steel. Int. J. Plast. 25, 183–204.

Maimí, P., Camanho, P., Mayugo, J., Turon, A., 2011. Matrix cracking and delamination in laminated composites. Part i: Ply constitutive law, first ply failure and onset of delamination. Mech. Mater. 43(4), 169–185.

Miehe, C., 1998. A constitutive frame of elastoplasticity at large strains based on the notion of a plastic metric. Int. J. Solids Struct. 35, 3859–3897.

Miehe, C., Apel, N., Lambrecht, M., 2002. Anisotropic additive plasticity in the logarithmic strain space: modular kinematic formulation and implementation based on incremental minimization principles for standard materials. Comput. Methods Appl. Mech.Eng. 191, 5383–5425.

v. Mises, R.V., 1928. Mechanik der plastischen Formänderung von Kristallen. ZAMM 8, 161–185.

Mosler, J., Bruhns, O., 2009. Towards variational constitutive updates for non-associative plasticity models at finite strain: models based on a volumetric-deviatoric split. Int. J. Solids Struct. 46, 1676–1684.

Naghdi, P., Trapp, J., 1975. The significance of formulating plasticity theory with reference to loading surfaces in strain space. Int. J. Eng. Sci. 13, 785–797.
Papadopoulos, P., Lu, J., 2001. On the formulation and numerical solution of problems in anisotropic finite plasticity. Comput. Methods Appl. Mech.Eng. 190, 4889–4910.
Pettermann, H., Planskensteiner, A., Böhm, H., Rammerstorfer, F., 1993. A thermo-elasto-plastic constitutive material law based on an incremental mori-tanaka approach. Comput. Struct. 71, 197–214.
Press, W., Teukolsky, S., Vetterling, W., Flannery, B., 1992. Numerical Recipes in Fortran. Cambridge University Press, Cambridge.
Rabotnov, J., 1969. Creep problems in Structural members, Vol. 7. North-Holland series in Applied Mathematics and Mechanics, North-Holland, Amsterdam, Netherlands.
Rogers, T., 1987. Yield criteria, flow rules and hardening in anisotropic plasticity. Boehler, Yielding, Damage and Failure of Anisotropic Solids, EGF publication 5, pp. 53–79.
Schröder, J., Gruttmann, F., Löblein, J., 2002. A simple orthotropic finite elasto-plasticity model based on generalized stress-strain measures. Comput. Mech. 30, 48–64.
Schuecker, C., Pettermann, H., 2008. Combining elastic brittle damage with plasticity to model the non-linear behavior of fiber reinforced laminates. Comput. Methods Appl. Sci. 10, 99–117.
Simó, J., Hughes, T., 2000. Computational Inelasticity. Mechanics and Materials, Springer.
Smith, J., Liu, W., Cao, J., 2015. A general anisotropic yield criterion for pressure-dependent materials. Int. J. Plast. 75, 2–21.
Smith, P., 2000. Carbon fiber reinforced plastics–Properties. In: Kelly, A., Zweben, C. (Eds.), Comprehensive Composite Materials. Pergamon, Oxford, pp. 107–150.
Spencer, A., 1992. Plasticity theory for fibre-reinforced composites. J. Eng. Math. 26, 107–118.
Sun, C., Chen, J., 1989. A simple flow rule for characterizing nonlinear behavior of fiber composite. J. Compos. Mater. 23, 1009–1020.
Totry, E., González, C., LLorca, J., 2008. Prediction of the failure locus of C/PEEK composites under transverse compression and longitudinal shear through computational micromechanics. Compos. Sci. Technol. 68 (15), 3128–3136.
Totry, E., Molina-Aldareguía, J., González, C., LLorca, J., 2010. Effect of fiber, matrix and interface properties on the in-plane shear deformation of carbon-fiber reinforced composites. Compos. Sci. Technol. 70 (6), 970–980.
Tsai, J., Sun, C., 2002. Constitutive model for high strain rate response of polymeric composites. Compos. Sci. Technol. 62 (10), 1289–1297.
Vogler, M., Rolfes, R., Camanho, P., 2013. Modeling the inelastic deformation and fracture of polymer composites - part i: plasticity model. Mech. Mater. 59, 50–64.
Vogler, T., Kyriakides, S., 1998. On the effect of loading rate on the compressive strength of an AS4/PEEK composite. J. Appl. Mech. ASME 65, 1056–1058.
Vogler, T., Kyriakides, S., 1999. Inelastic behavior of an AS4/PEEK composite under combined transverse compression and shear. Part i: experiments. Int. J. Plast. 15, 783–806.
Voyiadjis, G., Thiagarajan, G., 1995. An anisotropic yield surface model for directionally reinforced metal-matrix composites. Int. J. Plast. 11, 867–894.
Voyiadjis, G., Thiagarajan, G., 1996. A cyclic anisotropic-plasticity model for metal–matrix composites. Int. J. Plast. 12, 69–91.
Vyas, G., Pinho, S., Robinson, P., 2011. Constitutive modeling of unidirectional composites at the ply level using a plasticity-based approach. Compos. Sci. Technol. 78, 1068–1074.
Weeks, C., Sun, C., 1995. Nonlinear rate dependence of thick-section composite laminates. In: Rajapakse, Y.D.S., Vinson, J.R. (Eds.), High Strain Rate Effects on Polymer, Metal and Ceramic Matrix Composites and Other Advanced Materials, vol. 48. ASME, pp. 81–95.
Xie, M., Adams, D., 1995. A plasticity model for unidirectional composite materials and its applications in modeling composites testing. Compos. Sci. Technol. 27, 11–21.
Yun, G., Shang, S., 2011. A self-optimizing inverse analysis method for estimation of cyclic elasto-plasticity model parameters. Int. J. Plast. 27 (4), 576–595.
Zaïri, F., Naït-Abdelaziz, M., Gloaguen, J., Lefebvre, J., 2008. Modelling of the elasto-viscoplastic damage behaviour of glassy polymers. Int. J. Plast. 24 (6), 945–965.
Zheng, Q., 1994. Theory of representations for tensor functions - a unified invariant approach to constitutive equations. Appl. Mech. Rev. 47 (11), 545–586.
Zheng, Q., Spencer, A., 1993. Tensors which characterize anisotropies. Int. J. Eng. Sci. 31 (4), 679–693.

Swaroop G Nagaraja is a doctoral student in the Department of Polymer Science and Engineering at University of Leoben. He received a bachelor's degree in mechanical engineering from Bangalore University, India and a master's degree in computational mechanics from University of Stuttgart, Germany. His current field of research focuses on non-linear continuum mechanics and constitutive theories of inelasticity with application to fibre reinforced composite materials.

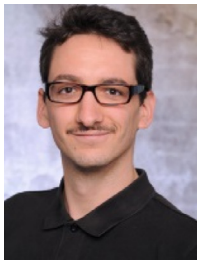

Martin Pletz studied Polymer Engineering and Science at Montanuniversitaet Leoben, Austria. He got his PhD in Material Science at the same university. He has been working in modelling and simulation for structural applications for 12 years in the fields of railway mechanics, electronics reliability and polymer engineering. In these fields, he has been modelling with metal, ceramic and polymer materials and methods such as contact mechanics, fracture mechanics and homogenization methods. He is working as a senior researcher at the chair of Designing Plastics and Composite Materials at the Montanuniversitaet Leoben.

Prof. Clara Schuecker obtained her PhD in Mechanical Engineering at the Vienna University of Technology, Austria. She has been working in the field of material modeling and structural simulation of composites for more than 20 Years both, as a researcher and a consultant to the aerospace industry. She received her tenure as full professor for Designing Plastics and Composite Materials at Montanuniversitaet Leoben in 2014. Her main field of research concerns the modeling of failure and damage in composites which she has been pursuing in collaboration with research groups at Syracuse University, Nasa Langley Research Center, and Imperial College London.